Influence of Na Content on the Chemical Stability of Nanometric Layered Na_xRhO_2 ($0.7 \leq x \leq 1.0$)

Aúrea Varela,[a] Marina Parras,[a] and José M. González-Calbet*[a]

Keywords: Na_xRhO_2 nanoparticles / Layered oxides / High resolution electron microscopy

A new Na_xRhO_2 solid solution composed of nanometric particles of the α-$NaFeO_2$ structural type has been stabilised in the $0.7 \leq x \leq 1$ range. Its rhombohedral structure is built from close packed layers of edge-sharing [RhO_6] octahedra separated by intercalant layers consisting of octahedrally coordinated Na. Electron microscopy shows that compositional variations are indeed accommodated by means of stacking faults leading to a local change in the Na oxygen environment. Samples are air-sensitive, and the aged materials partially decompose, segregating sodium carbonate.

Introduction

AMO_2 layered oxides (A: alkaline, M: transition metal) have been widely studied because of their interesting physical properties.[1–5] Among them, Na_xCoO_2 has attracted particular interest due to the large thermoelectric power of the metallic conductor $NaCo_2O_4$[6–7] and the recent discovery of superconductivity near 4 K in hydrated $Na_{0.3}CoO_2{\cdot}1.3H_2O$.[8,9]

The structures of various Na_xCoO_2 phases have been reported. All of them are based on the stacking of CoO_2 layers, consisting of edge-sharing CoO_6 octahedra. The Na atoms form layers between the CoO_2 layers. $NaCoO_2$ (x = 1) crystallises in the α-$NaFeO_2$ structure.[10] This rock-salt type structure is built from a cubic stacking of oxygen layers (*ABCABC*) with Co and Na occupying the octahedral sites of alternating layers.[11] A decrease in the Na content changes the Na coordination from octahedral to trigonal prism, leading to the stabilisation of different structures.[10] Moreover, a recent electron diffraction study of various Na_xCoO_2 ($0.15 < x < 0.75$) compositions has shown the existence of several ordered distributions of the Na vacancies that lead to a wide range of superstructures of the basic hexagonal cell depending on the x value.[12]

The discovery of superconductivity in the cobalt oxyhydrate $Na_{0.3}CoO_2{\cdot}1.3H_2O$[8,9] spread the interest in this system. From a structural point of view, the oxyhydrate phases are formed by CoO_2 layers stacked together with one layer of Na^+ ions and two layers of water molecules. The insulating layers, which alternate with the CoO_2 layers, play the dual role of spacing provider and redox controller. In addition to this superconducting phase, a series of hydrated phases have been stabilised for the same Na/Co ratio, the H_2O content ranging from $Na_{0.3}CoO_2{\cdot}1.4H_2O$ to $Na_{0.3}CoO_2$.[13] In this work, Foo et al. studied the influence of Na and H_2O contents on the structural and physical properties of these compounds.

Much less attention has been devoted to 4d or 5d metal oxides. Among them, the ruthenium oxides have probably been the most studied because they exhibit a rich variety of magnetic and electrical properties.[14,15] Recently the structural characterisation of the new layered oxide $NaRuO_2$ and and oxyhydrate $Na_{0.22}RuO_2{\cdot}0.45H_2O$ have been reported but no superconducting behaviour has been observed in the hydrated phase.[16]

Rhodium oxides have also been studied recently, and a new sodium rhodate, $NaRh_2O_4$, has been stabilised under high pressure.[17] This compound crystallises in the $CaFe_2O_4$ structure, which is a 3-D structure comprising a network of edge-sharing RhO_6 octahedra. In addition to this 3-D material, layered $NaRhO_2$ has been reported by K. Hobbie et al.[18] The structural refinement carried out on a single crystal shows this compound to be isostructural to α-$NaFeO_2$. However, unlike the aforementioned Na_xCoO_2 system, where compositional variations have been extensively studied, only $NaRhO_2$ is known in the Na_xRhO_2 series. The present work is devoted to the systematic investigation of the compositional variations of the Na_xRhO_2 system and its structural and microstructural characterisation.

Results and Discussion

Chemical and Structural Characterisation

The Na:Rh cationic ratio, determined as described in the experimental section, is shown in Table 1. The Na content depends on both the time of the thermal treatment and the

[a] Departamento de Química Inorgánica, Facultad de Químicas, Universidad Complutense,
28040 Madrid, Spain
Fax: +34-91-394-43-52
E-mail: jgcalbet@quim.ucm.es

container used. Our results indicate that Na loss is favoured by long thermal times and by the use of Al_2O_3 crucibles.

Table 1. Preparation conditions of the Na_xRhO_2 samples.

Label	Crucible	Annealing time [h]	Chemical composition[a]
PT-24	Pt	24	$NaRhO_2$
PT-48	Pt	48	$Na_{0.85}RhO_2$
AL-24	Al_2O_3	24	$Na_{0.7}RhO_2$
AL-48	Al_2O_3	48	phase mixture[b]

[a] The estimated error in cationic composition is around 2%. [b] Hydrated and non-hydrated $NaRhO_2$ phases.

Na_xRhO_2 ($1 \geq x \geq 0.7$) samples were characterised by means of XRD. The pattern corresponding to $NaRhO_2$ (PT-24) is shown in Figure 1a. All maxima can be indexed on the basis of a rhombohedral unit cell (R-3m) of parameters a = 3.0903(1) and c = 15.5400(6) Å. The pattern has been refined by the Rietveld method by taking as the starting model the structural data of the isostructural α-$NaFeO_2$. The graphic result of this refinement can be seen in Figure 1a. Table 2 lists the refined structural parameters and selected interatomic distances are shown in Table 3. The crystallographic data obtained are in agreement with those previously reported for a $NaRhO_2$ single crystal.[18]

The XRD pattern corresponding to $Na_{0.85}RhO_2$ (PT-48), Figure 1b, is very similar to that of stoichiometric $NaRhO_2$. The only visible difference is that (00l) reflections are shifted toward lower 2θ values, indicating a slight increase in the c-axis length. Actually, the obtained cell parameters correspond to a = 3.0867(6), c = 15.5785(5) Å. The structure was refined in the R-3m space group, by using the $NaRhO_2$ structure model with a reduced Na content of 0.85 per unit formula, according to cationic analysis. The graphic result of this refinement is shown in Figure 1b, while Figure 2 depicts the crystal-structure view of $Na_{0.85}RhO_2$. As it can be observed, the structural features of stoichiometric $NaRhO_2$ are maintained. The rhombohedral structure is formed by close-packed layers of edge-sharing [RhO_6] octahedra perpendicular to the c-axis separated by intercalant Na layers, Na also being octahedrally

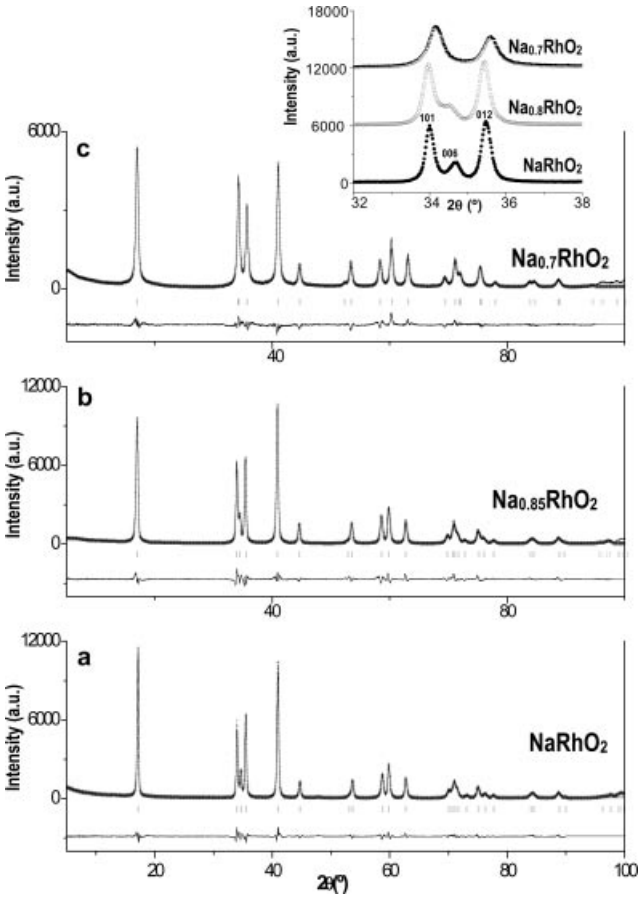

Figure 1. Experimental, calculated and difference powder XRD patterns corresponding to Na_xRhO_2 samples. (a) x = 1 (PT-24); (b) x = 0.85 (PT-48) and (c) x = 0.70 (AL-24). An enlargement of a portion of the XRD patterns is shown in the inset.

Table 2. Structural parameters of Na_xRhO_2 ($0 \leq x \leq 0.7$).

$NaRhO_2$ (PT-24)						
Atom	Site	x	y	z	Occ.	B [Å^2]
Rh	3b	0	0	0.5	1.0	0.28(1)
Na	3a	0	0	0	1.0	0.59(1)
O	6c	0	0	0.232(3)	1.0	0.31
a = 3.0903(1) Å, c = 15.5400(6) Å; R_B = 2.34, R_{exp} = 4.37, R_{wp} = 10.6, χ^2 = 5.84						
$Na_{0.85}RhO_2$ (PT-48)						
Atom	Site	x	y	z	Occ.	B [Å^2]
Rh	3b	0	0	0.5	1.0	0.11(8)
Na	3a	0	0	0	0.86(1)	0.08(2)
O	6c	0	0	0.234(2)	1.0	0.1(9)
a = 3.0867(6) Å, c = 15.5781(1) Å; R_B = 3.52, R_{exp} = 5.08, R_{wp} = 12.8, χ^2 = 6.3						
$Na_{0.7}RhO_2$ (AL-24)						
Atom	Site	x	y	z	Occ.	B [Å^2]
Rh	3b	0	0	0.5	1.0	0.17(1)
Na	3a	0	0	0	0.71(1)	0.94(2)
O	6c	0	0	0.230(3)	1.0	0.721(9)
a = 3.0750(3) Å, c = 15.766(1) Å; R_B = 6.34, R_{exp} = 4.97, R_{wp} = 10.34, χ^2 = 4.39						

Table 3. Selected interatomic distances [Å] in Na_xRhO_2 ($0.7 \leq x \leq 1$).

	$NaRhO_2$	$Na_{0.85}RhO_2$	$Na_{0.7}RhO_2$
Rh–O	2.058(2)	2.069(2)	2.027(2)
Na–O	2.372(3)	2.358(3)	2.422(3)
Rh–Rh	3.090	3.090	3.075
Na–Na	3.090	3.090	3.075
Rh–Na	3.145	3.145	3.171

coordinated to the oxygen atoms. The refined structural parameters and some selected interatomic distances are listed in Table 2 and Table 3, respectively.

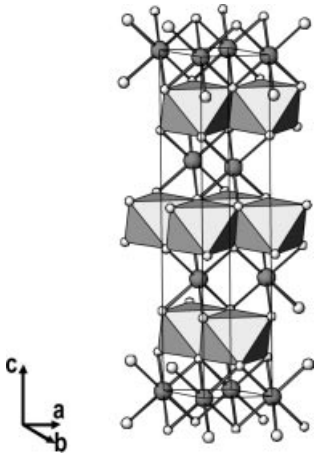

Figure 2. Crystal structure of $Na_{0.85}RhO_2$. Grey dots correspond to sodium and small dots to oxygen atoms.

It is well known that XRD is not the most powerful technique to study structural effects of light atoms such as oxygen or sodium. However, the refinement was stable, and it was possible to refine the Na fractional occupancy. The obtained value, corresponding to a Na content of 0.86 atoms per unit formula, nicely agrees with the cationic analysis. Moreover, the lack of extra maxima in the XRD patterns indicates a random distribution of the Na vacancies through the intercalant layers. The metal-oxygen distances correspond to 2.069(2) and 2.358(3) Å for Rh–O and Na–O, respectively, both comparable with their typical values.[17,18]

According to these results, the decrease in the Na concentration from $NaRhO_2$ occurs only with minor structural changes. The *c* parameter increases, indicating a slight increase in the thickness of the intercalant Na layers. Furthermore, a small shrinkage of the *a*-axis is also observed. The shrinking of the RhO_2 layers is probably due to the partial oxidation of Rh(III) to Rh(IV), which occurs in order to ensure charge neutralisation when Na ions are removed.

The above features are more pronounced in $Na_{0.7}RhO_2$ (AL-24), which also presents the structural characteristics of stoichiometric $NaRhO_2$. The corresponding structure has also been refined by the Rietveld method (Figure 1c), and the refined lattice parameters, a = 3.0750(2), c = 15.766(1) Å (see Table 2), show again the expansion of the *c*-axis as well as the contraction of the *a*-axis when Na content decreases. As a consequence, (101) and (006) reflections overlap, and only one diffraction maximum is observed (see inset of Figure 1). These structural features are also reflected in the corresponding interionic distances. Actually, as it can be seen in Table 3, the Na–Rh distance increases from 3.14 for $NaRhO_2$ to 3.17 Å for $Na_{0.7}RhO_2$. In addition, the Rh–O distance decreases from 2.058(2) to 2.0269(5) Å, because of the smaller size of Rh^{IV} ($r_{Rh^{IV}}$ = 0.60; $r_{Rh^{III}}$ = 0.65 Å in an octahedral environment[19]).

Similar behaviour has been previously observed in the Na_xCoO_2 system.[13] The *c*-axis is increased from 10.82 Å, for the stoichiometric $NaCoO_2$ (x = 0), to 11.23 Å for x = 0.3. A series of hydrated phases has recently been reported for this Na content.[8,20,21] The lower hydrate, $Na_{0.3}CoO_2{\cdot}0.6H_2O$, has a *c*-parameter of 13.8 Å that corresponds to an expansion of 1.3 Å per intercalant layer as compared to $Na_{0.3}CoO_2$. The H_2O molecules are found in the same plane as the Na atoms, unlike the model proposed for superconducting $Na_{0.3}CoO_2{\cdot}1.4H_2O$[8] in which the *c*-parameter is increased to 19.6 Å. This value corresponds to an expansion of 2.8 Å per intercalant layer, and, in this case, Na ions and H_2O molecules are not located in the same plane.

In Na_xRhO_2, the *c*-axis value increases from 15.540 for x = 1 to 15.766 Å for x = 0.7. This small expansion seems to indicate that, up to x = 0.7, the Na^+ ions lost into the intercalant layers are not replaced by H_2O molecules. However, to fully discard this possibility a thermogravimetric analysis of the above samples has been performed.

The weight change of PT-24, PT-48 and AL-24 samples, when heated at 0.2 °C/min in flowing O_2 in a thermogravimetric analyser (TGA), is presented in Figure 3. No substantial weight loss occurs over the temperature range of 30 to 300 °C. Actually, if we consider that the observed weight loss (close to 0.2%) corresponds to H_2O molecules, a content of only 0.02 water molecules per unit formula should be obtained. These results seem to indicate that down to 0.7-mol Na content, H_2O molecules are not introduced into the layer space, at least not in a significant amount.

A different result is obtained when the sample is treated at 800 °C for 48 h in alumina crucibles (AL-48). The corresponding XRD pattern is shown in Figure 4a. The main peaks of this pattern can be also indexed on the basis of the above-described rhombohedral unit cell with lattice parameters close to a = 3.09, c = 15.7 Å; however, extra maxima of very low intensity are also visible (marked in the figure with asterisks). This sample is air-sensitive, and, after 24 h in air, the intensities of the extra maxima increase (Figure 4b). This fact has also been reported for the isostructural $NaRuO_2$.[12] Actually, this compound is also air-sensitive, and, after one night in air, an oxyhydrate is formed with the stoichiometry $Na_{0.22}RuO_2{\cdot}0.45H_2O$. Therefore, the extra peaks of Figure 4 could correspond to a new $Na_xRhO_2{\cdot}yH_2O$ hydrate. In fact, all these maxima can be indexed on the basis of a rhombohedral unit cell of parameters a = 3.02, c = 20.46 Å. The high value of the *c*-axis should be a consequence of the intercalation of some H_2O molecules. Unfortunately, this oxyhydrate phase has

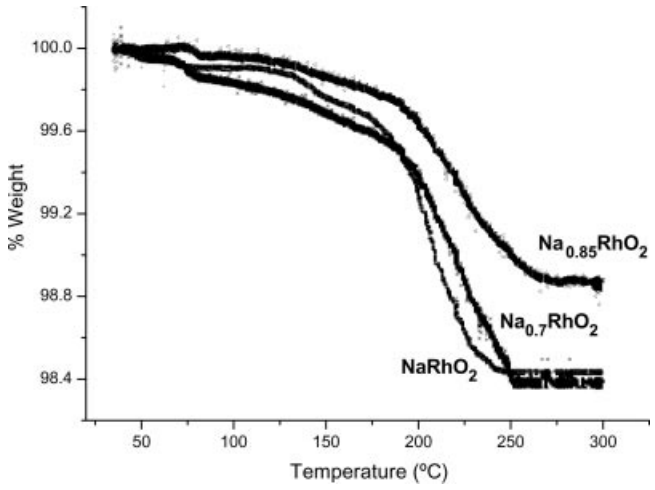

Figure 3. Thermogravimetric curves of Na_xRhO_2 samples ($1 \leq x \leq 0.7$). Experiments were carried out in O_2 for a ~100 mg specimen with a heating rate of 0.2 °C/min.

not been isolated up to now. Finally, it is worth recalling that this hydration process is highly reversible, and, after 1 hour at 800 °C in air, the non-hydrated phase is already stabilised (see Figure 4c).

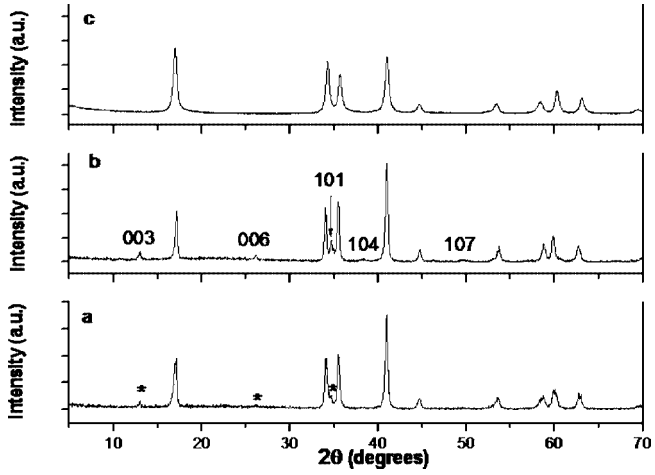

Figure 4. Experimental powder XRD patterns corresponding to (a) sample AL-48; (b) sample AL-48 after being aged 24 h in air and (c) the previous sample heated for 1 h at 800 °C in air.

As described above, the Na content of the samples varies, depending on the preparation conditions, from 1.0 to 0.7 mol per unit formula. Recently, Zandbergen et al.[12] have studied the Na_xCoO_2 system by electron diffraction. They have shown the existence of an extensive series of superstructures of the basic $NaCoO_2$ structure originating from different ordered distributions of the Na vacancies. In order to study the influence of the Na content in the microstructure of the Na–Rh–O system, a study by selected area electron diffraction (SAED) and high resolution electron microscopy (HREM) has been carried out.

Figure 5a corresponds to the SAED pattern of stoichiometric $NaRhO_2$ (PT-24) along the [010] zone axis. All the observed crystals show the same pattern. The local composition, analysed by energy-dispersive X-ray spectroscopy (EDS), nicely agrees with the experimental composition. All the spots appearing in the pattern can be indexed on the basis of the rhombohedral unit cell with parameters $a \approx 3.8$, $c \approx 15.6$ Å, which are in agreement with the XRD results. Moreover, the lack of streaking along the c^* axis is evidence of an ordered situation as confirmed by HREM. The HREM image along [010] (Figure 5b) shows a fully ordered material with interplanar distances of 2.7 and 15.6 Å, corresponding to d_{100} and d_{001}, respectively. The optical Fourier transform (inset in the figure) shows features similar to the experimental SAED pattern in Figure 5a. An enlargement of the image is depicted in Figure 5c. The observed differences can be associated to the atomic configuration shown in the structural model projection depicted in Figure 5c. The brightest dots are attributed to Rh atoms forming the ABCABC stacking sequence, which corresponds to the 3R structure. The dots of intermediate intensity correspond to the lighter Na and O atoms. The calculated image for $\Delta t = 7$ nm, $\Delta f = -60$ nm, shown in the inset, nicely fits the experimental data. All observed crystals have the same features, and no stacking faults are observed.

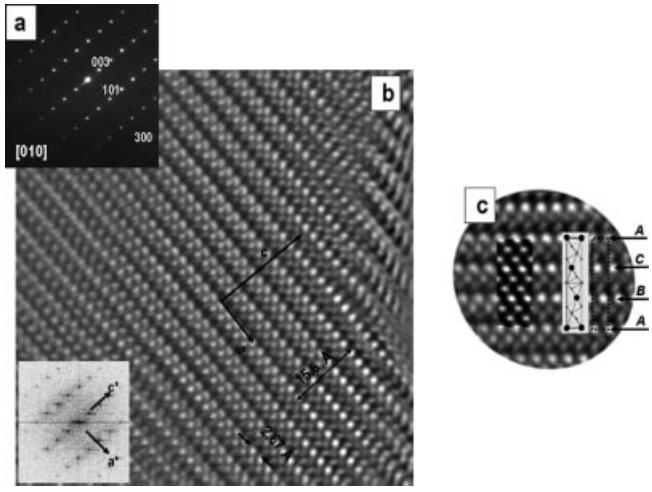

Figure 5. (a) SAED pattern corresponding to $NaRhO_2$ along [010]. (b) Corresponding HREM image. The Optical Fourier Transform and the calculated image are shown in the insets. (c) Enlargement of the above image. The unit cell shows the ...*ACB*... stacking sequence characteristic of the $NaRhO_2$ structure. The calculated image is shown in the inset. Big dots correspond to Rh, grey dots to Na and small black dots to oxygen atoms.

It is worth recalling that, under electron beam irradiation, crystals are unstable. Actually, Figure 6a and b shows the SAED pattern and the corresponding HREM, along [010], of a $NaRhO_2$ crystal after an extended period of electron beam illumination. Radical changes were observed and the microstructure was altered in such a way that some kind of disorder appeared, as evidenced by the presence of streaking along the c^*-axis (see Figure 6a). The corresponding HREM shows the presence of stacking faults along the crystal. These faults locally change the stacking of the 3R-$NaRhO_2$ phase by the incorporation of one A-layer in the ABC cubic sequence, giving rise to a local change in the

Na sites from octahedral to trigonal prismatic. The electron damage is more important for thinner crystals. For this reason, in order to obtain images such as the ones in Figure 5, low exposure times should be used and crystals that are not too thin must be chosen.

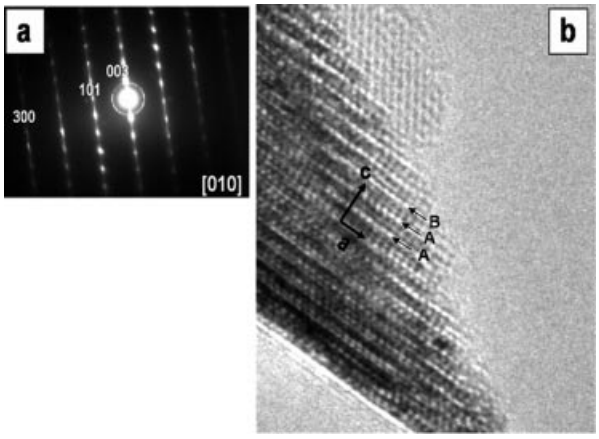

Figure 6. (a) SAED pattern corresponding to $NaRhO_2$ along [010] after electron beam irradiation. Streaking along the *c*-axis is apparent. (b) Corresponding HREM image showing stacking faults.

TEM characterisation of Na_xRhO_2 samples reveals a disordered stacking sequence apparent in the SAED pattern (Figure 7a) as diffuse streaking along the *c** axis, as well as in the corresponding image (Figure 7b) as planar defects. Note that the same disordered microstructure of Na-deficient materials is observed for stoichiometric $NaRhO_2$ under long beam time exposure. It seems that the electron beam favours the diffusion of Na out of the irradiated area, generating local Na-deficient areas with a disordered microstructure.

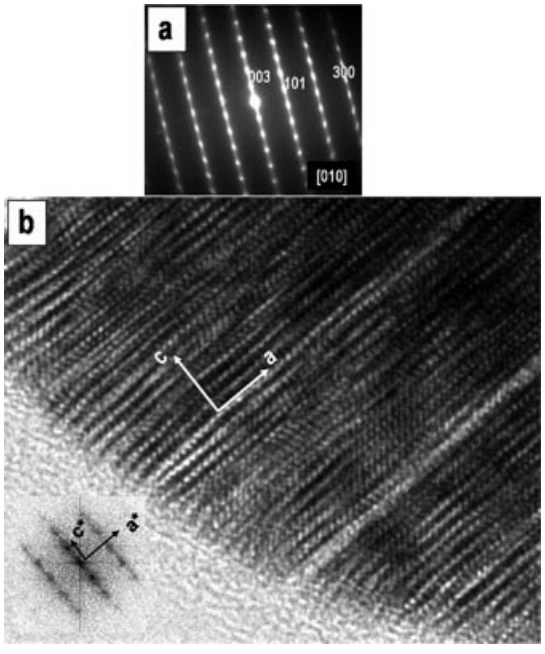

Figure 7. (a) SAED pattern corresponding to Na_xRhO_2 along [010]. (b) Corresponding HREM image.

Morphological Characterisation

In order to study the dependence of the morphology of the Na_xRhO_2 samples ($0.7 \leq x \leq 1$) on the duration of the thermal treatment and the crucibles used, a SEM characterisation was performed. Figure 8a–d shows SEM micrographs of the Na_xRhO_2 samples heated for 24 (24-PT) and 48 h (48-PT) in Pt (a, b), and for 24 (24-AL) and 48 h (48-AL) in Al_2O_3 (c,d) containers. All samples exhibit a similar platelike morphology with a quite homogeneous size distribution (100–200 nm). These small particles form agglomerates of around 1–2 μm. The powders obtained exhibit a partially sintered microstructure due to a certain degree of particle coarsening and sintering. All of the studied samples show analogous features. This fact seems to indicate that neither the thermal treatment nor the container used plays an important role in the morphology and crystallinity of the samples.

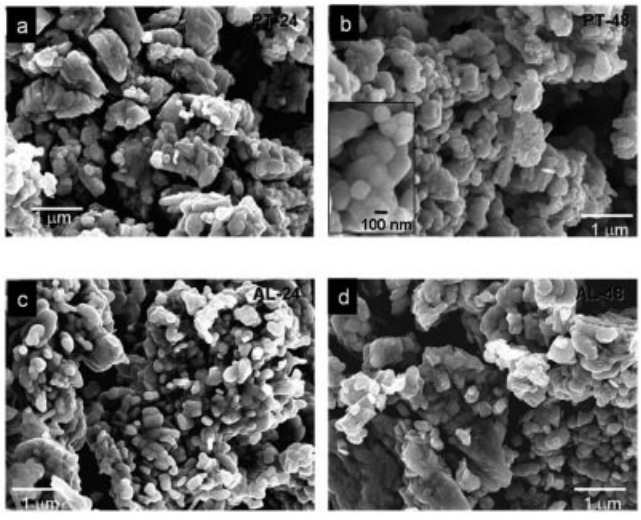

Figure 8. SEM micrographs of the Na_xRhO_2 samples heated at 800 °C, 24 and 48 h in Pt (a, b) and 24 and 48 h in Al_2O_3 (c,d) containers. Sintered microstructure of the nanoparticles can be observed in the enlargement of (b).

In addition to the morphology, SEM characterisation has evidenced an important common feature of these samples. Although the samples are carefully stored in a dry box, their morphology markedly changes with the aging time. Figure 9 corresponds to the $NaRhO_2$ sample (PT-24) 15 (a) and 30 (b) days after being prepared. It is clearly visible that, besides the platelike particles characteristic of $NaRhO_2$, needlelike particles (2–3 μm) appear to some extent. Both the amount as well as the particle size of these needles gradually increases with the aging time. In fact, these particles grow up to around 6 μm after 30 days, whereas the size of the platelike particles remains constant. The EDS analysis carried out on the needles indicates the presence of C and Na, but no Rh is detected. It follows that these particles should correspond to a minor phase of sodium carbonate segregated when the material is aged. At this stage, we have studied these samples by XRD. The XRD patterns of the aged samples are not different from a

freshly prepared sample. Neither extra maxima nor intensity changes of the maxima are detected. This result, corroborated by electron diffraction, suggests that the segregated sodium carbonate is a noncrystalline phase. The decomposition process progresses over time and, after several months, it is visible in the XRD patterns by the appearance of broadened diffraction maxima corresponding to a hydrated and poorly crystalline sample. The other Na_xRhO_2 (x = 0.85, 0.7) samples undergo the same aging process.

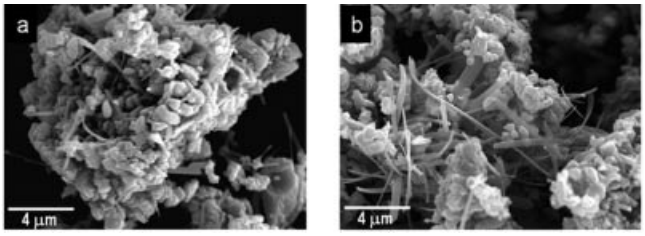

Figure 9. SEM micrographs of $NaRhO_2$ (PT-24): (a) 15 and (b) 30 days after preparation.

Concluding Remarks

On the basis of the XRD results, it can be concluded that a Na_xRhO_2 solid solution with the α-$NaFeO_2$ structure is stable in the $0.7 \leq x \leq 1$ compositional range. The relative disposition of the CoO_6 sheets is kept, and therefore no significant modifications in the Na environment are observed. In fact, in this compositional range, the main structural features of stoichiometric $NaRhO_2$ are maintained, and only a variation of the lattice parameters is observed. Finally, whereas no water is incorporated in the $0.7 \leq x \leq 1$ range, a hydrated phase appears for $x < 0.7$, which has not been isolated to date.

According to SAED and HREM results, variations in the amount of Na in Na_xRhO_2 are not totally randomly distributed throughout the crystal as indicated by XRD. In fact, the decrease in Na content gives rise to a local change in the stacking sequence of the RhO_2 sheets, leading to Na in a trigonal prism environment. However, no long-range order was attained, and no new ordered phases were stabilised in the compositional range studied. In this respect, the situation is different from the Na_xCoO_2 system,[12] where several structures have been stabilised as a function of the Na content. In this way, we would like to emphasize that, in spite of the presence of a significant Na vacancy concentration, none of the prepared samples show Na ion conductivity.

Finally, the morphological characterisation shows that all freshly prepared samples are composed of nanometric particles (100–200 nm) with the same platelike shape. In addition, all Na_xRhO_2 ($0.7 \leq x \leq 1$) samples are air-sensitive: the aging process leads to a final stage in which deliquescence takes place, and the sample decomposes, segregating sodium carbonate.

Experimental Section

Samples were prepared as polycrystalline powders by the solid state reaction of Na_2CO_3 and Rh_2O_3 in a 1:1 ratio with heating at 800 °C in flowing oxygen. It is well known that, during the synthesis process, Na can be lost because of the high volatility of Na_2O. Therefore, in order to obtain materials with various Na:Rh ratios, different annealing times as well as different crucibles were used.

The Na:Rh cationic ratio was determined on pellet samples by microprobe analysis with a JSEM-8600 scanning electron microscope working at an acceleration voltage of 10 KV. In addition, the local composition was analysed by EDS with an INCA analyser system attached to a JEOL 3000 FEG electron microscope.

To determine the precise water content of the samples, a thermal study was carried out with a high-sensitivity thermobalance (CAHN D-200) by heating in oxygen a specimen of around 80 mg up to 300 °C at a rate of 0.2 °C/min. This electrobalance allows the detection of weight variations within $\pm 5 \times 10^{-3}$ mg in a sample of about 100 mg.

Powder X-ray diffraction (XRD) patterns were collected using Cu-K_α radiation (λ = 1.5418 Å) at room temperature with a PHILIPS X′PERT diffractometer equipped with a graphite monochromator. Diffraction data were analysed by the Rietveld method,[22] using the Fullprof program.[23]

The samples were characterised by SAED and HREM with a JEOL 3000 FEG electron microscope fitted with a double-tilting goniometer stage (±22°, ±22°). Simulated HREM images were calculated by the multislice method using the MacTempas software package. The morphological study was carried out with a JSM-6330F FEG scanning electron microscope working at 10 kV.

Acknowledgments

Financial support through research projects MAT2004–01248 and MAT/0627/2004 are acknowledged

[1] J. R. Dahn, U. V. Sacken, C. A. Michel, *Solid State Ionics* **1990**, *44*, 87–97.
[2] K. Mizushima, P. C. Jones, P.-J. Wiseman, J. Goodenough, *Mater. Res. Bull.* **1980**, *15*, 783–789.
[3] M. M. Thackeray, *Prog. Solid State Chem.* **1997**, *25*, 1–71.
[4] J. M. Tarascon, M. Armand, *Nature* **2001**, *414*, 359–367.
[5] C. Delmas, *Mater. Sci. Eng.* **1989**, *B3*, 97–101.
[6] I. Terasaki, Y. Sasago, K. Uchinokura, *Phys. Rev. B* **1997**, *56*, R12685–12687.
[7] I. Terasaki, Y. Ishii, D. Tanaka, Y. Iguchi, *Jpn. J. Appl. Phys.* **2001**, *40*, L65–67.
[8] K. Takada, H. Sakurai, E. Takayama-Muromachi, F. Izumi, R. A. Dilanian, T. Sasald, *Nature* **2003**, *422*, 53–55.
[9] R. E. Schaak, T. Klimczuk, M. L. Foo, R. J. Cava, *Nature* **2003**, *424*, 527–529.
[10] C. Delmas, C. Fouassier, P. Hagenmuller, *Physica* **1980**, *B99*, 81–85.
[11] C. Fouassier, G. Matejka, J. M. Reau, P. Hagenmuller, *J. Solid State Chem.* **1973**, *6*, 532–537.
[12] H. W. Zandbergen, M. Foo, Q. Xu, V. Kumar, R. J. Cava, *Phys. Rev. B.* **2004**, *70*, 024101–024108.
[13] M. Foo, R. E. Schaak, V. L. Miller, T. Klimczuk, N. S. Rogado, Y. Wang, G. C. Lau, C. Craley, H. W. Zandbergen, N. P. Ong, R. J. Cava, *Solid State Commun.* **2003**, *127*, 33–37.
[14] Y. Maeno, H. Hashimoto, K. Yoshida, S. Nishizaki, T. Fujita, J. G. Berdnorz, F. Lichtenberg, *Nature* **1994**, *372*, 532–534.
[15] G. Cao, S. McCall, F. Freibert, M. Shepard, P. Henning, J. E. Crow, *Phys. Rev. B* **1996**, *53*, 12215–12219.

[16] M. Shikano, C. Delmas, J. Darriet, *Inorg. Chem.* **2004**, *43*, 1214–1216.
[17] K. Yamaura, Q. Huang, M. Moldovan, D. Young, A. Satro, Y. Baba, T. Nagai, Y. Matsui, E. Takayama-Muromachi, *Chem. Mater.* **2005**, *17*, 359–365.
[18] K. Hobbie, R. Hoppe, *Z. Anorg. Allg. Chem.* **1988**, *505*, 106–110.
[19] R. D. Shanon, *Acta Crystallogr.* **1976**, *32*, 751–767.
[20] D. P. Chen, H. C. Chen, A. Maljuk, A. Kulakov, H. Zhang, P. Lemmens, C. T. Lin, *Phys. Rev. B* **2004**, *70*, 0245061–0245068.
[21] M. Karppinen, I. Asako, T. Mohashi, H. Yamuchi, *Chem. Mater.* **2004**, *16*, 1693–1696.
[22] H. V. J. Rietveld, *J. Appl. Crystallogr.* **1969**, *2*, 65–71.
[23] J. Rodríguez-Carvajal, *Physica B* **1993**, *192*, 55–69.

Received: May 19, 2005
Published Online: September 15, 2005

